Numerical Method for Calculation of Surface Tension Flows in Arbitrary Grids

P. Y. Liang*
Rockwell International/Rocketdyne Division, Canoga Park, California 91303

This paper outlines a scheme to define and track interfaces in an arbitrary quadrilateral grid by making use of a single fractional volume of fluid (VOF) variable to describe the distribution of the liquid phase in a gas-liquid-particles flowfield. The present methodology, however, represents a substantial refinement over the original VOF programs in that nonorthogonal, body-fitted, and even deforming grids can be used, and the gas and liquid phases can take on totally different properties, including compressibility and incompressibility. The interface is unambiguously defined; it either forms a closed loop or terminates at boundaries with specified wall adhesion angles. Then, local curvatures can be estimated and surface-tension forces determined and applied to the acceleration of local velocities. Furthermore, the availability of the interface orientations with respect to the computational cell boundaries enables a higher-order estimate of the appropriate volume of liquid (as vs gas) that is to be fluxed across a cell boundary. The rewards for this added sophistication are superior liquid contiguity and shape preservation properties compared with simpler interface tracking methods. Examples demonstrating the versatility of the code in two-phase flow applications are presented.

Introduction

IN fluids engineering, there are numerous situations where it is important to resolve the dynamics of the interfaces separating two immiscible fluids. Applications include vehicular tank slosh analysis, low-gravity space applications, lubrication analysis, atomizing jets, droplet/spray dynamics, and two-phase flows in chemical processes. In computational fluid dynamics, there are two basic approaches to the tracking of free surfaces. The first approach uses Lagrangian-type methods, such as putting markers on the interface or using grids that deform with the heavier fluid.[1-3] It has the advantage of circumventing the problem of numerical diffusion across the interface. However, the methods become inapplicable whenever the deformation of the interface is severe, such as in drop or liquid jet breakup studies. In such circumstances, the utility of the Lagrangian methods may be extended to a limited degree by the restructuring of the grid or redistribution of the markers. This strategy was adopted by Fyfe et al.[4] However, such undertakings inevitably involve great complexity in bookkeeping and reintroduce numerical diffusion, which the Lagrangian methods are intended to avoid in the first place. These Lagrangian tracking methods can be used in conjuction with a global Eulerian grid for the fluid field variables.

The second approach seeks to retain the numerical versatility of a purely Eulerian representation. Then, to track an interface that arbitrarily intersects the grid, an additional field variable is introduced whose value indicates the relative absence or presence of each of the immiscible fluids within a computational cell. The exact location and orientation of the interface is then inferred based on the local magnitude and distribution of this variable. One commonly used variable is the fractional volume of one of the fluids, as in the volume of fluid (VOF)[5] scheme. To minimize numerical diffusion, special treatments are necessary when evaluating the advection of this particular variable. Nichols et al.[6] use a variation of the donor-acceptor concept, which implicitly assumes that the interface is either normal to or parallel to the local advection velocity. A concise overview of the advantages and disadvantages of the different methods has been presented by Laskey et al.,[7] who classified the approaches slightly differently according to whether the surface itself is tracked, or just reconstructed when required, or a simple Lagrangian grid is used (thus effectively tracking the surface also). The method presented in this paper is an extension of the VOF philosophy. The fundamental difference lies in the fact that actual "watermark" coordinates are defined from the VOF variable at each time step and that these watermarks are joined together by line segments to form a continuous curve representing the interface instead of a set of disconnected segments as in the original VOF scheme. Thus, the location and orientation of the interface is uniquely defined in space and does not change when the computational scheme sweeps the Eulerian grid in different directions. At first sight, the scheme thus appears similar to the surface tracking or combination Lagrangian-Eulerian methods, but in actuality this is not so, as the surface coordinates are *not* advected, they are only reconstructed at each new time step. All necessary information is still contained in one single VOF variable, thereby preserving the simplicity of the VOF approach. Accordingly, the resolution power of the scheme is also limited to one coordinate point per computational cell.

Once defined, the position of the interface is used for two purposes: 1) calculation of surface curvature for determining surface tension forces and 2) partitioning of the flux terms across cell boundaries into two portions, each representing a different fluid.

The advantages of the present method over the conventional VOF scheme are summarized in Table 1. They stem primarily from the unambiguous definition of the interface. The scheme has been implemented into the advanced rocket injector combustion code-surface tracking (ARICC-ST) version of the ARICC[8] code, which is a general purpose multiphase combustion code derived from the CONCHAS-SPRAY[9] code by combining the latter's three-step implicit continuous Eulerian (ICE) Navier-Stokes solver and discrete particle technique with the VOF concept. Before describing the interface tracking algorithm, a brief summary is first given about the ARICC three-phase computational environment under which tracking is performed. The reader is referred to

Received Sept. 9, 1988; revision received Dec. 21, 1989. Copyright © 1990 by the American Institute of Aeronautics and Astronautics, Inc. All rights reserved.

*Member, Technical Staff, Advanced Combustion Devices. Member AIAA.

Table 1 Comparison of the SOLA-volume of fluid and ARICC-ST surface tracking scheme

SOLA-Volume of Fluid	ARICC-ST
Rectangular grid	Arbitrary quadrilaterals
Fixed grid	Rezonable grid
Ambiguous definition of interface location and orientation	Unambiguous definition of watermark coordinates
Nonconnecting surface segments	Contiguous surface segments
Fluids of equal acoustic seeds only	Gas and liquid phases of totally independent properties including sound speeds
Advection of F based on donor or acceptor values	Advection of F based on actual interface location
Linear velocity profile across interface	Bilinear or higher-order velocity profile across interface to account for different μ_g and μ_ℓ
Uniform distribution of surface cell mass to momentum cells	Preferential distribution of surface cell mass
Adhesion to vertical or horizontal walls	Adhesion to arbitrarily oriented walls, including sharp corners

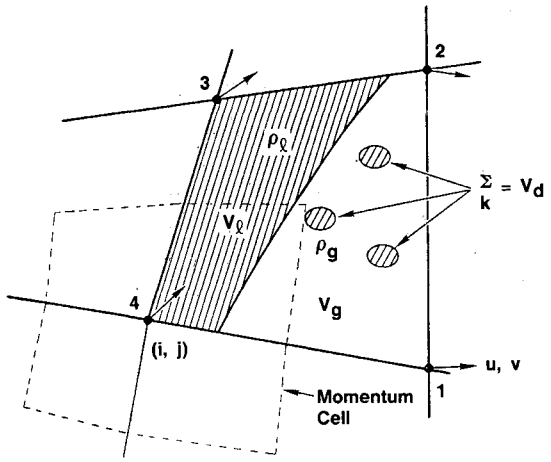

Fig. 1 General computational volume in the ARICC scheme.

Ref. 8 for details. All discussion in this paper is restricted to two-dimensional axisymmetric cases, although the concepts are readily extended to three-dimensions.

Basic ARICC Methodology

ARICC was developed for the purpose of simulating combustion flows where a thick spray and atomizing jets are involved, such as in liquid propellant rocket combustion chambers. Because of substantial volumetric displacement by each of the three (liquid, gas, droplets) phases, a strong dynamic coupling exists among them, and each phase needs to be resolved independently. To achieve this, the standard finite volume formulation is modified as follows:

1) Partitioning the computational control volume into multiple subvolumes (see Fig. 1). In the most general case, portions of the cell are occupied by each of the three phases. Two additional variables are introduced to keep track of the relative volumetric fractions as well as areal blockages by the droplets. Droplets are treated as discrete Lagrangian particles, whereas the liquid or gas are continuum media and finite-differenced accordingly. For the purposes of this paper, only the liquid and gas phases are of concern. The corresponding VOF variable is defined as

$$F = V_g/(V_g + V_\ell) \tag{1}$$

2) Pressure coupling between gas and liquid phases. To retain simplicity in cells where both liquid and gas phases are present, a single value of pressure is still defined for the entire cell. (An exception is when the gas phase is replaced by a vacuum or an "inert" medium of given constant pressure. See next section.) The liquid is considered to be incompressible or nearly incompressible, whereas the gas is treated as fully compressible. Thus, when a control volume is compressed, all of the compression is assumed to take place over the gaseous subvolume. Such a "compound" fluid can take on interesting new properties, some of which are discussed by Liang,[10] such as an effective sound speed that is lower than either that of the liquid or of the gas.

3) Mass and momentum exchange between the phases. Semiempirical physical submodels appearing as source terms in the conservation equations are used to account for interphase transport, such as the conversion of the liquid into droplets or vapor or vice versa. (These correspond to the physical processes of atomization, evaporation, and their inverse processes.) If desirable, energy exchange can likewise be modeled. Momentum exchange between the gas and liquid, however, is implicitly treated. Following the practice of CONCHAS-SPRAY, momentum cells are constructed around the regular cell vertices where the velocities are defined (see Fig. 1). Volumetrically, the regular cell is partitioned by joining the cell's center with the cell face midpoints, with each portion contributing to each of the four associated momentum cells. However, when the liquid and gas residing within the same regular cell are of vastly different densities (typically of the order of 10^2 times different), the apportioning of the regular cell's mass, and hence momentum, to the four vertices becomes an issue. In the baseline ARICC scheme, a homogeneous, averaged density is assumed:

$$\bar{\rho} = \rho_g F + \rho_\ell (1 - F) \tag{2}$$

as in a single-phase calculation. This scheme works, but substantial numerical diffusion in momentum results, producing the effect of excessive interface drag. To improve upon this situation, the regular cell's mass must be preferentially distributed, which, in turn, requires knowledge about the interface location and orientation. To this end, a refined free-surface tracking scheme is developed, and it is to this scheme we now turn.

Approach for Interface Tracking Scheme

Figure 2 depicts the major steps involved in defining the interface and utilizing the additional information thereby made available. They are explained briefly below.

Step 1 Cell Linkage Determination

A global sweep over the mesh is first conducted to determine which of the cells are viable candidate interface-containing cells (surface cells), namely, those cells that have $0 \le F < 1$ and have at least one empty (purely gaseous) cell out of its eight neighbors. In general, any cell can take on

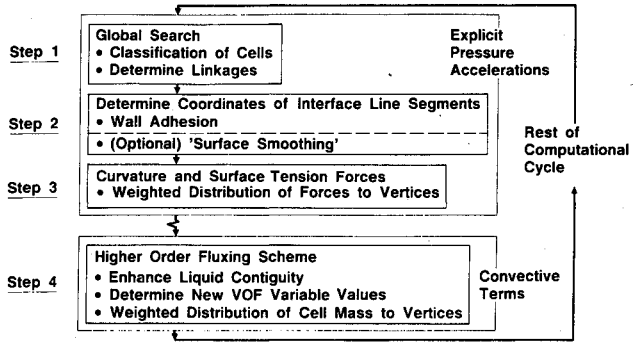

Fig. 2 Flowchart showing the free-surface tracking scheme within the ARICC-ST code computational cycle.

fractional F values, but not all of them should be allowed to be a surface cell. Note that cells with $F = 0$ are included; it is possible for a cell lying on the surface of a liquid region to be completely filled with liquid.

Then a search is initiated with any surface cell, but priority is given to those that are either next to a wall or an axis of symmetry *and* have the largest number of empty (purely gaseous) neighbors. To proceed with the search, the following rules are postulated.

1) Only two surface cells with a common cell face can be linked together.

2) A surface must either form a complete closed loop or terminate at a boundary.

3) A cell cannot be crossed by a surface more than once. Consequently, a surface cannot reverse on or cross itself.

4) If a cell can be linked to more than one neighbor, it is assumed that the linkage continues in the same direction as the previous segment.

5) Whenever a search path reaches a dead end, it backtracks until a cell offers a possible alternative path, and the search continues from there. All previously tried surface cells are then declared noncandidates.

6) When a surface cannot be extended further, except to cross itself, the search may be successfully terminated with the surface forming a closed loop. Any "dangling branches" of the initial portion of the surface will be eliminated and the cells returned to candidate status.

Step 1 is repeated until all candidate cells have been exhausted and all possible surface loops have been formed. The linkage information is stored in two additional arrays, giving the forward and backward links for each true surface cell.

Figure 3 gives examples of different liquid shapes and the corresponding linkages. It is evident that small liquid fragments will not necessarily be resolved as independent regions, but may be left out in the freestream or included as part of a larger region.

Step 2 Watermark Coordinates

A watermark location is defined for each surface cell. For two-dimensional quadrilateral grids, cell linkages can only be one of two kinds: a straight link, or a left or right turn (see Fig. 4). If it is the former, a "fathom line" is constructed linking the midpoints of the two cell edges that the interface does not intersect. If it is the latter, the fathom line is a diagonal approximately normal to the interface. Then, a watermark is chosen along this fathom line such that, if a line segment perpendicular to the fathom line and passing through the watermark is drawn, it partitions the cell into liquid and gas subvolumes that correspond approximately to the correct F value. It is only approximate because the arbitrary quadrilateral is treated either as a trapezoid (for straight links), or as a trapezoid plus two triangles (see Fig. 5). However, the volume calculations do take into account whether the grid is a two-dimensional planar one or an axisymmetric one.

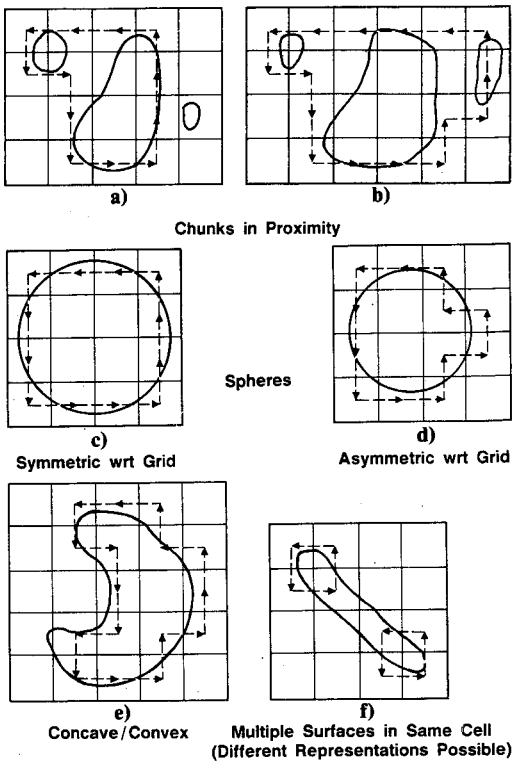

Fig. 3 Examples of different liquid shapes and corresponding cell linkages.

Once defined, the watermarks can be joined together to give an unambiguous and physically realistic representation of the interface. If the interface terminates at a wall, the last segment of the interface is constructed so as to produce the proper wall adhesion angle (an input property). Finally, an optional smoothing scheme is also included to smooth out small unphysical wriggles.

Step 3 Calculation of Surface Tension

Surface-tension evaluation is based on the curvature K_{arc} of a circular arc passing through a watermark and its two adjacent neighbors. The surface-tension pressure always points toward the center of curvature and is given by

$$P_s = -\sigma K \tag{3}$$

where

$$K = K_{\text{arc}} + K_{\text{cyl}} = \frac{1}{R_{\text{arc}}} + \frac{1}{R_{\text{cyl}}} \tag{4}$$

The second right-hand-side term of Eq. (4) is 0 for planar grids. P_s is assumed to act over an area A_s from $[(X_M + X_{M-1})/2, (Y_M + Y_{M-1})/2]$ to $[(X_M + X_{M+1})/2, (Y_M + Y_{M+1})/2]$, where subscript M denotes the watermark in question.

One more issue remains. The force $f_s = P_s A_s$ is a cell-centered quantity that must be distributed to the four corner vertices (unlike the thermodynamic pressure, which acts over a distinctive area associated with each of the momentum cells). If the cell contents were homogeneous, the force should be distributed in proportion to the volume contributed by the regular cell to each of the four momentum cells. Since the cell contents are not homogeneous, however, and the liquid and gas densities are hugely different, a set of weighting factors reflecting the concentration of cell mass toward the heavier fluid is superimposed on top of the volumetric weighting factors, i.e.,

$$f_{s_i} = f_s \times W_i / \Sigma W_i \tag{5}$$

where

$$W_i = W_{m_i} \times W_{v_i}, \qquad i = 1, 2, 3, 4$$

and W_v are proportional to the volumes of the momentum cell quadrants. A similar set of compound weighting factors is used in apportioning the cell mass to the four corners. The prescription for W_m is discussed next.

Step 4 Weighted Mass Distribution and Higher-Order Fluxing Scheme

To avoid undue algebraic complexity, even for a two-dimensional situation, no attempt is made to actually solve for the multiple intersections of the interface with the momentum cell boundaries. The preferential distribution of fluid mass within a cell is thus only qualitatively approximated. Formulas of varying complexity can be prescribed for the weighting factors provided that

1) All weights are equal when the cell is fully gaseous or fully liquid.

2) The greatest difference in the weights result when the cell is half-filled.

3) The formulas are symmetrical with respect to the position of the fluid. That is, if the liquid and gas swap positions without moving the interface, the respective weights would also swap position.

An example of the weight formulas is given in Table 2. Because of the symmetry property, the reader should be able to derive the complete set of formulas when the relative orientation of the fluids is different.

The unambiguous definition of an interface location not only enables the weighted distribution of mass and surface-tension forces within a cell, but also makes it possible to account for a nonlinear velocity profile across the interface between two vertices. In Fig. 6, the velocity profile associated with the left face of the cell, which intersects the interface, is assumed to be made up of two linear segments joining at the intersection point. Balance of viscous forces requires that the slopes of the two segments bear the relationship

$$\mu_g \times \frac{(U_3 - U_s)}{(X_3 - X_s)} = \mu_\ell \times \frac{(U_s - U_4)}{(X_s - X_4)} \tag{6}$$

which can be used to solve for U_s. Equation (6) may be replaced with a more sophisticated profile shape function if so desired. The two shaded regions add up to the total volume flux across the left face, each corresponding to the gaseous volume flux and the liquid volume flux, respectively. In the ARICC-ST implementation, as a further refinement, the intersection point S is determined using the average of the old time and (estimated) new time locations of the interface, advected based on U_3 and U_4. For the bottom and top faces of the cell, which the interface does not intersect, a linear velocity profile is assumed, and the effective F value used for the fluxing calculation in that case is chosen as

$$\bar{F} = \max(F_D, F_A) \tag{7a}$$

if fluxing from inside of liquid region

$$\bar{F} = \min(F_D, F_A) \tag{7b}$$

if fluxing from outside of liquid region

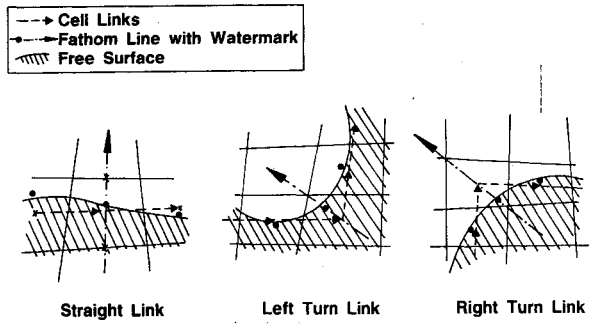

Fig. 4 Definitions of fathom lines and watermarks in a surface cell.

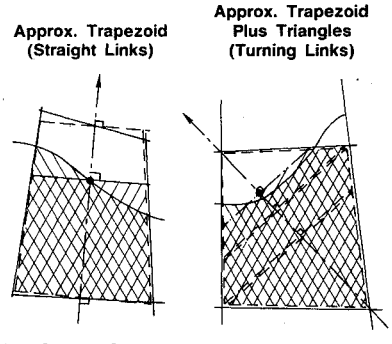

Fig. 5 Liquid and gas volume partitioning for arbitrary quadrilaterals.

Table 2 Examples of weight formulas and distribution of surface cell mass to momentum vertices

	Straight link	Left turn link
	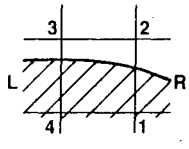	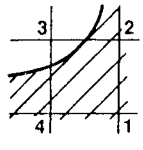
W_{m_1}	where $W_B = 0.5\,\rho_\ell - \max(F - 0.5, 0)(\rho_\ell - \rho_g)$, $W_R = 1 + \frac{F_L}{F_L + F_R} \cdot \frac{\lvert W_B - W_T \rvert}{W_B + W_T}$, $W = W_B \cdot W_R$	$0.25(\rho_\ell + \rho_g) + (0.75 - \max(0.5, F))(\rho_\ell - \rho_g)$
W_{m_2}	where $W_T = 0.5\,\rho_g + \max(0.5 - F, 0)(\rho_\ell - \rho_g)$, $W = W_T \cdot W_R$	$0.25(\rho_\ell + \rho_g) - \{\min[\max(F, 0.25), 0.75] - 0.5\}(\rho_\ell - \rho_g)$
W_{m_3}	where $W_L = 1 + \frac{F_R}{F_R + F_L} \cdot \frac{\lvert W_B - W_T \rvert}{W_B + W_T}$, $W = W_T \cdot W_L$	$0.25(\rho_\ell + \rho_g) + [\min(0.5, F) - 0.25](\rho_\ell - \rho_g)$
W_{m_4}	$W_B \cdot W_L$	W_{m_2}

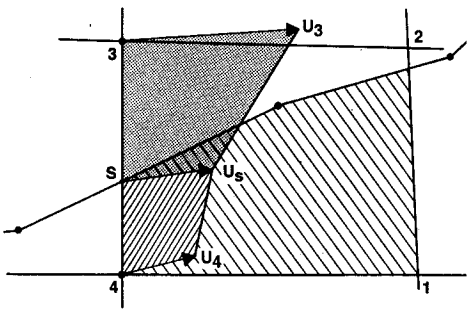

Fig. 6 Bilinear velocity profile across an interface and corresponding fluxing volumes.

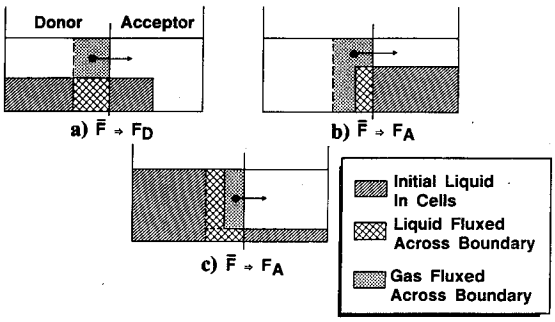

Fig. 7 Limiting fluxes of gas and liquid volumes across cell boundaries (dashed line indicates boundary of total volume fluxed).

where the subscripts D and A refer to the "donor" and "acceptor" cells on either side of the cell face.

Flux Limiters

The preceding fluxing scheme implied that a nonupwind value of F is used in evaluating the convective terms. Thus, flux limiters must be imposed to prevent more gas or liquid than is available to be fluxed out of the donor cell. This is done as follows:

$$\Delta V_\ell = \min[(1-\bar{F})\,\Delta V_{\text{total}} + \mathscr{F},\ V_{\ell,D}] \tag{8}$$

and

$$\mathscr{F} = \max(0,\ \bar{F}\cdot\Delta V_{\text{total}} - V_{g,D}) \tag{9}$$

where

$$\min(F_D, F_A) \le \bar{F} \le \max(F_D, F_A)$$

The situation is schematically depicted in Fig. 7. Equation (8) prevents more liquid than is available to be fluxed, and Eq. (9) does the same for the gas.

Cutoff Value for F

Because of truncational errors or other sources of noise, it is possible that tiny "fragments" of liquid be dispersed over a gaseous region or vice versa. To prevent these from unreasonably distorting or complicating the interface shape, as well as to avert numerical difficulties when tiny gas pockets are trapped within a largely liquid cell, cutoff values of F must be prescribed so that we set

$$F \to 0 \quad \text{if} \quad F < F_{\text{cut}} \tag{10a}$$

$$F \to 1 \quad \text{if} \quad F > 1 - F_{\text{cut}} \tag{10b}$$

One dynamic way of defining F_{cut} is

$$F_{\text{cut}} = \max\left\{\min\left[1\times10^{-3}, \frac{\max(|\Delta V_{\ell,N}|, |\Delta V_{\ell,S}|, |\Delta V_{\ell,E}|, |\Delta V_{\ell,W}|)}{2\times V_{\text{cell}}}\right] \times 1\times10^{-5}\right\} \tag{11}$$

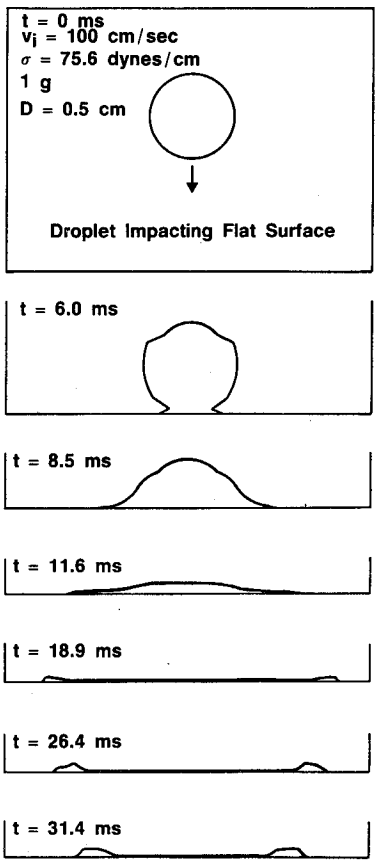

Fig. 8 Drop falling through vacuum and impacting hard surface.

The idea is that F_{cut} is as large as accuracy considerations should allow (10^{-3} or 0.1% of cell volume is an insignificant amount of liquid), but not so large that even if liquid is being fluxed into an initially empty cell, the liquid will be wiped out by this cutoff value. On the other hand, F_{cut} cannot be zero, therefore a lower limit of 10^{-5} is used.

Pressure Interpolation for Vacuum Ambient

In the event that the gaseous phase is replaced with a vacuum or an inert medium of prescribed pressure, the pressure boundary condition must be imposed at the free surface. Since the thermodynamic pressure is normally defined at the cell center, it is obtained through linear interpolation between the surface and an interpolation cell inside the liquid region. The interpolation cell is chosen from among the surface cell's eight neighbors based on the linkage information, so that the line joining its center and the center of the surface cell is pretty much normal to the interface. Then

$$P_{ij} = (1-\eta)P_N = \eta P_{\text{surf}} \tag{12}$$

where

P_{ij} = the surface cell-centered pressure
P_N = the interpolation cell-centered pressure
P_{surf} = the given surface pressure

and $\eta = d_c/d$ is the ratio of the distance between the cell centers, and the distance between the watermark and the interpolation cell center. Equation (12) must be applied throughout the iterative calculation process for the pressure acceleration. If the surface cell undergoes compression, for example, its center moves and d_c changes, even though d does not.

Examples

It may be pointed out that even though the scheme seems quite complicated, the additional computational load is still manageable. The reason is that, for most applications, the number of surface cells is small compared with the computational grid. The following examples demonstrate the versatility of the scheme.

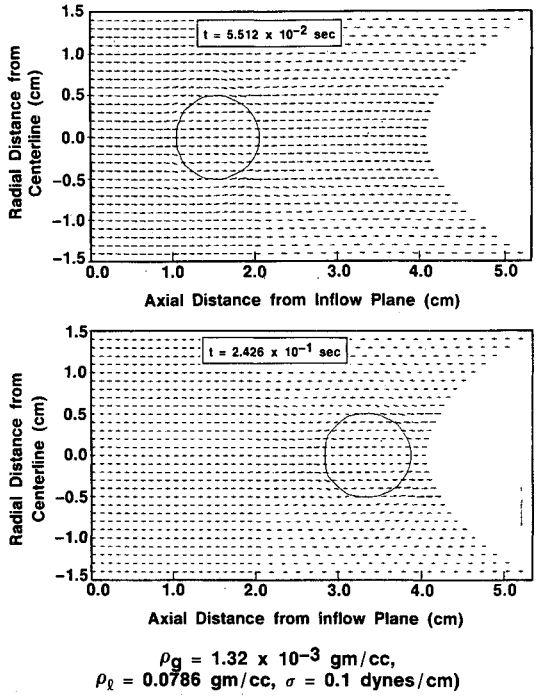

Fig. 9 Translation of spherical drop through nonrectangular grid.

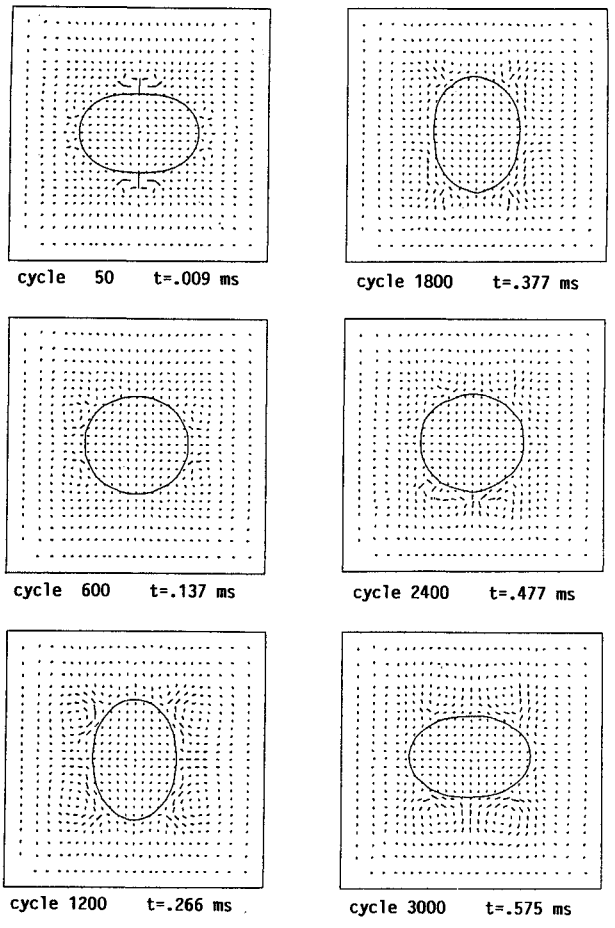

Fig. 10 Normal mode oscillation of simulated kerosene droplet.

Drop Falling through Vacuum

Figure 8 shows a water drop of 0.5 cm diam falling with 100 cm/s initial velocity in a 1-g gravity field. Because of the short falling distance (0.65 cm), there is no appreciable acceleration, and impact velocity is insufficient to cause the drop to shatter. The case demonstrates the scheme's ability to work with a vacuum ambient. After impact, the liquid spreads out onto a thin film, but surface tension eventually stops the spread and causes the overshot liquid to collect back toward the center. Maximum spread diameter is about 1.63 cm at 18.9 ms.

Translation of Liquid Region

The preceding example utilized a simple rectangular (though nonuniform) grid. One advantage of actually determining the watermark coordinates to represent the location of an interface is that the interface definition will not be a strong function of the cell shapes, and hence arbitrary quadrilaterals can be used. (There is still some weak dependence, so long as the interface itself is not tracked, but only inferred from the VOF variable.) Figure 9 demonstrates this capability. Both the circular liquid region (1 cm diam) and the surrounding air is moving from left to right at a constant speed of 10 cm/s. The liquid starts out in a zone with rectangular grids, but gradually moves into a zone with increasingly skewed cells (as reflected in the location of the velocity vectors). Generally speaking, the shape-preservation ability of the scheme has held up quite well. There are some minor distortions, but they are traced more to noise generated in the velocity field rather than to the surface tracking scheme itself. Refinements are being developed to further reduce the spurious perturbations, which get more noticeable as the density ratio between the liquid and gas becomes huge and when the Eulerian velocity of the liquid is substantial. Under those circumstances, momentum transfer from the liquid to the gas will have a big impact on the gas velocity.

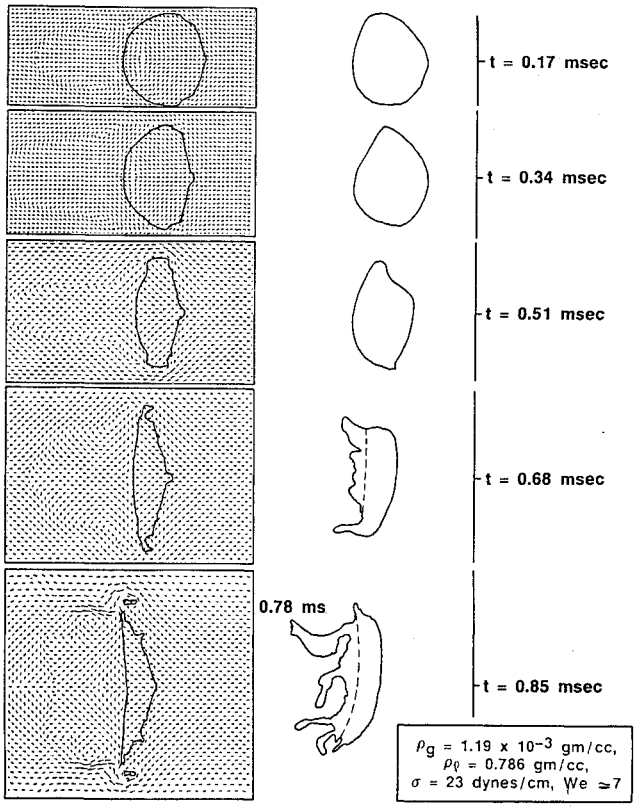

Fig. 11 Deformation and shear mode breakup of droplet under cross flow.

Normal Mode Droplet Oscillation

A frequently used test case for surface-tension schemes is that of a droplet undergoing normal mode oscillation. With a large density ratio between the liquid and the surrounding gas, such a problem represents a stringent test on the validity of the method. One such calculation using a Lagrangian grid is reported by Fyfe et al.,[11] who also extended the linear theory for the oscillation period to include the presence of an external fluid

$$\omega_n^2 = (n^3 - n)\frac{\sigma}{(\rho_\ell + \rho_g)r_d^3} \tag{13}$$

where

$n = 2$ for the lowest mode
r_d = droplet radius (two-dimensional "drop")
σ = surface tension.

In Fig. 10, a simulation using the current scheme is presented for a kerosene droplet ($\rho_\ell = 0.82$ g/cc) in air ($\rho_g = 1.3 \times 10^{-3}$ g/cm^3). The drop radius is 0.0125 cm and $\sigma = 30$ dynes/cm. The period, as determined from the computer plots, is approximately 6×10^{-4} s (cycle 3200), compared with the theoretical value of 5.9×10^{-4} s and the results by Fyfe et al. of 7.1×10^{-4} s. The grid size used was 26×26, with 14×10 cells inside the droplet initially.

Droplet Breakup Studies

In the final example, we show the results of an important application to the study of the breakup of a droplet under the shearing effects of a convective stream. The breakup of propellant droplets has been studied experimentally[12] and is believed to be an important controlling factor in the combustion rate of liquid rocket engine chambers. Figure 11 shows an initially stationary (1200 μ) droplet of kerosene being subjected to an instantaneous flowfield of air of 3.38×10^3 cm/s (established by sending a shock wave of appriate strength into the system). The computer-generated droplet shapes are compared with the experimental results found in Ref. 12. As the flow evolves, a lengthening wake and the drop's internal circulation develop. The drop flattens out as expected, and eventually sheds off ligaments around the outer rim. Since droplet deformation is the result of a delicate balance among viscous, surface tension, and pressure forces, the good qualitative agreement testifies to the basic validity of the scheme. The details of this and other related cases were presented and discussed in a separate paper.[13]

Concluding Remarks

The full range of the current scheme's potential is yet to be explored. Several issues, such as the challenges of dealing with extreme density ratios between liquid and gas, of handling complicated interface geometries especially when liquid fragmentation occurs, and of further refining the velocity profile across the interface in the surface cell, remain to be investigated. For example, when the distribution of liquid regions is dispersed or fragmentary, it is conceivable that sudden changes in surface shapes can still occur numerically, with attending abrupt redistribution of vertex masses and momentum and surface-tension forces. While every effort has been made to make the search scheme as "smart" as possible, this problem, which is basically one of resolution, has not been totally overcome. On the other hand, relatively straightforward upgrades of the current scheme, such as adding evaporation and heat transfer between the liquid and the gas, and liquid interior heat transfer, will permit direct simulations of droplet evaporation and combustion, etc., hitherto impossible. These possibilities are currently being pursued.

Acknowledgments

The author wishes to thank A. Gharakhani and V. Young for their assistance in carrying out some of the computations cited in the examples.

References

[1]Welch, J. E., Harlow, F. H., Shannon, J. P., and Daly, B. J., "The MAC Method: A Computing Technique for Solving Viscous Incompressible, Transient Fluid-Flow Problems Involving Free Surfaces," Los Alamos Scientific Lab. Rept. LA-3425, Los Alamos, NM, March 1966.

[2]Nichols, B. D., and Hirt, C. W., "Improved Free-Surface Boundary Conditions for Numerical Incompressible Flow Calculations," *Journal of Computational Physics*, Vol. 8, No. 3, 1971, pp. 434–448.

[3]Hirt, C. W., Cook, J. L., and Butler, T. P., "A Lagrangian Method for Calculating the Dynamics of an Incompressible Fluid with Free Surface," *Journal of Computational Physics*, Vol. 5, No. 2, 1970, pp. 103–124.

[4]Fyfe, D. E., Oran, E. S., and Fritts, M. J., "Numerical Simulation of Droplet Oscillations, Breakup, and Distortion," AIAA Paper 87-0539, Jan. 1987.

[5]Hirt, C. W., and Nichols, B. D., "Volume of Fluid (VOF) Method for the Dynamics of Free Boundaries," *Journal of Computational Physics*, Vol. 39, No. 1, 1981, pp. 201–225.

[6]Nichols, B. D., Hirt, C. W., and Hotchkiss, R. S., "SOLA-VOF: A Solution Algorithm for Transient Fluid Flow with Multiple Free Boundaries," Los Alamos Scientific Lab. Rept. LA-8355, Los Alamos, NM, Aug. 1980.

[7]Laskey, K. J., Oran, E. S., and Boris, J. P., "The Gradient Method for Interface Tracking," Naval Research Lab., Washington, DC, 1987.

[8]Liang, P. Y., Fischer, S., and Chang, Y. M., "Comprehensive Modeling of a Liquid Rocket Combustion Chamber," *Journal of Propulsion and Power*, Vol. 2, No. 2, 1986, pp. 97–104.

[9]Cloutman, L. D., Dukowicz, J. K., Ramshaw, J. D., and Amsden, A. A., "CONCHAS-SPRAY; A Computer Code for Reactive Flows with Fuel Spray," Los Alamos Scientific Lab. Rept. LA-9294-MS, May 1982.

[10]Liang, P. Y., "Analysis of Coaxial Spray Combustion Flames and Related Numerical Issues," AIAA Paper 86-1511, June 1986.

[11]Fyfe, D. E., Oran, E. S., and Fritts, M. J., "Surface Tension and Viscosity with Lagrangian Hydrodynamics on a Triangular Mesh," *Journal of Computational Physics*, Vol. 76, No. 2, 1988, pp. 349–384.

[12]Rabin, E., and Lawhead, R., "The Motion and Shattering of Burning and Non-burning Droplets," Air Force Office of Scientific Research, TN-59-129, Washington, DC, March 1959.

[13]Liang, P. Y., Gharakhani, A., and Eastes, T., "Computer Simulation of Drop Deformation and Drop Breakup," AIAA Paper 88-3142, Washington, DC, July 1988.